RSC Advances

PAPER

View Article Online
View Journal | View Issue

Cite this: *RSC Adv.*, 2024, **14**, 25301

Polyhedral oligomeric silsesquioxane (POSS)-silicon/carbon quantum dots nanocomposites for cell imaging†

Hai Liang,‡[a] Fan Wu,‡[b] Runan Xia,[a] Wei Wu,[a] Shiqi Li,[b] Panpan Di[a] and Miao Yang*[a]

Silicon quantum dots (SiQDs) and carbon quantum dots (CQDs) are renowned for their outstanding applications in fluorescence imaging and biosensing. However, their small size poses significant challenges in terms of preparation, collection, and purification. Polyhedral oligomeric silsesquioxanes (POSS), an organic-inorganic nanohybrid with a cage-like structure, has recently attracted considerable attention due to its excellent biocompatibility. In this research, we utilize the encapsulating properties of POSS to improve the optical property of SiQDs/CQDs through an *in situ* synthesis strategy, resulting in the production of blue-emitting POSS-SiQDs, green-emitting POSS-G-CNDs, and red-emitting POSS-R-CNDs. By examining their structural and optical characteristics, it is found that these hybrid materials exhibit excellent luminescent properties, biocompatibility and cell membrane permeability. This facilitates multicolor intracellular imaging and underscores their successful application in biological imaging. Our study presents a novel approach to synthesize POSS-QDs composite nanomaterials with new perspectives in biological imaging and medical diagnostics.

Received 22nd April 2024
Accepted 20th July 2024

DOI: 10.1039/d4ra02987a

rsc.li/rsc-advances

1. Introduction

Silicon quantum dots (SiQDs) and carbon quantum dots (CQDs) have revealed significant advancements in their applications for cellular fluorescence imaging. These advancements primarily utilize their optical properties, biocompatibility, and adaptability within biological environments.[1–6] SiQDs and CQDs have been synthesized with improved biocompatibility and functionalization capabilities, rendering them suitable for both *in vivo* and *in vitro* applications, devoid of the toxicity typically associated with traditional quantum dots like CdSe or InP.[7] For instance, Terada *et al.* developed multi-emissive SiQDs capable of emitting light in various colors, which enhances their utility in multiplexed imaging. This capability allows for simultaneous tracking of different cellular components or processes, providing a comprehensive understanding of cellular functions and interactions.[1] Wei *et al.* reported that functionalized SiQDs, such as those with sulfhydryl groups, exhibit high quantum yields and can specifically target cellular structures or reactive species, aiding precise imaging and sensing.[8]

Recent approaches in the synthesis of CQDs have embraced eco-friendly methods, such as deriving CQDs from plant sources. These plant-derived CQDs exhibit improved biocompatibility and solubility, making them ideal for biological applications.[9] Researchers have developed their utilization in real-time tracking and imaging of intracellular processes, which are crucial for diagnostics and cellular studies.[10] The ability to fine-tune the luminescent properties of CQDs through various doping and surface modification strategies has been particularly noted. For example, Ramasamy *et al.* demonstrated that integrating nitrogen during CQD synthesis, leads to the development of biocompatible markers. These nitrogen-infused CQDs have proven effective for cellular imaging applications, providing essential insights into cellular dynamics and morphology.[11]

Polyhedral oligomeric silsesquioxane (POSS) nanoparticles, as unique inorganic-organic hybrid materials, are composed of a silicon-oxygen core surrounded by organic groups.[12–15] This unique structure not only endows POSS nanoparticles with excellent mechanical and thermal stability but also enhances their chemical versatility, making them widely applicable in various fields such as biomedical imaging, catalysis, and composite material fabrication.[16,17] Moreover, through surface functionalization, POSS nanoparticles can carry specific biomarkers or fluorescent groups for cell labelling and tracking.[18] They also demonstrate good biocompatibility and adjustable biodegradability, making them especially useful in long-term imaging and targeted delivery systems.

[a]*Department of Pharmacy, The People's Hospital of Bozhou, Bozhou, Anhui Province, China. E-mail: smileivy2345@163.com*

[b]*School of Physics and Optoelectronic Engineering, Anhui University, Hefei, 230601, Anhui, P. R. China*

† Electronic supplementary information (ESI) available. See DOI: https://doi.org/10.1039/d4ra02987a

‡ These authors contribute equally.

The combination of POSS nanoparticles, CQDs, and SiQDs in cell imaging can bring widespread applications. This multifunctional nanocomposite material will not only enhance fluorescence properties, improving imaging quality, but also improves the material's biocompatibility and stability, reducing potential bio-toxicity.[5,19,20] This composite can be tailored for targeted imaging of specific cells or tissues, significantly enhancing specificity and accuracy. In the study of sensor and biomarker development,[21] these materials demonstrate great promise for monitoring and tracking specific molecules or biological processes within cells. In terms of drug delivery and treatment,[22,23] it offers potent avenues for more effective targeted therapies, while also allowing for the monitoring of drug release and distribution *via* advanced fluorescence imaging techniques. However, the common approach of separately synthesizing the two QDs and then physically mixing them with POSS. This does not effectively passivate the defects on the surface of the QDs, nor does significantly enhance their optical performance.

In this study, we *in situ* synthesized POSS with SiQDs and CQDs, using the unique structure of POSS to encapsulate and purify them, thereby preparing blue-emitting POSS-SiQDs, green-emitting POSS-G-CNDs, and red-emitting POSS-R-CNDs, respectively. Extensive analyses of these composites in terms of their structure, morphology, composition, and fluorescence properties demonstrated that they possess fine luminescent efficiency, short fluorescence lifetimes, satisfactory biocompatibility, and effective cell membrane permeability. These characteristics enable multicolour intracellular imaging, and the composites have been successfully implemented in biological imaging. Our research has proposed a novel strategy for composite nanomaterials, offering new perspectives for biological imaging and medical diagnostics.

2. Experimental section

PEG-POSS, perylene, formamide, natural red, potassium persulfate, 3-[2-(2-aminoethylamino)ethylamino]propyltrimethoxysilane (AEEA), ethylene glycol (EG) were bought from the Macklin. Capan_1 cells were bought from the Procell.

2.1 Synthesis of POSS-SiQDs

Initially, 0.22 g of PEG-POSS and 0.12 g of bengal red, 4 mL AEEA were dissolved in 16 mL of water.[24] The mixture was transferred into a 10 mL polytetrafluoroethylene-lined autoclave, sealed, and maintained at 160 °C for 4 hours. After cooling to room temperature, the solution was concentrated and purified. The final product was collected *via* freeze-drying and stored at 4 °C for future use.

2.2 Synthesis of POSS-G-CQDs

POSS-G-CQDs are synthesized utilizing a modified radical-assisted method.[25] In a standard procedure, 0.2 g of PEG-POSS, 0.375 g of perylene, and 0.4 g of potassium persulfate were combined in a 50 mL formamide solution. The mixture was heated to 80 °C for 30 minutes to facilitate the formation of POSS-G-CQDs. Upon completion, the mixture was allowed to cool to room temperature. The solution was then concentrated and purified.

2.3 Synthesis of POSS-R-CQDs

Red fluorescent POSS-R-CQDs were synthesized by adapting a previously reported procedure with modification.[26] Initially, 0.45 g of PEG-POSS and 0.4 g of natural red were dissolved in 10 mL of EG, and the mixture was stirred at 50 °C for 30 minutes. This solution was then transferred to a 50 mL glass-lined autoclave and heated to 200 °C, with the temperature of the reaction solution directly monitored. Afterward, the vessel was set aside to cool, and the product was collected. The purification process involved multiple washing and centrifugation steps to remove unreacted precursors.

2.4 Characterization

Transmission electron micrographs (TEM) were obtained using the JEM-2100 (JEOL). Powder X-ray diffraction (XRD) measurements were conducted on a SmartLab 9kw. Absorption spectra were recorded with a Shimadzu UV3600 (Japan). Fluorescence spectra were measured using a Hitachi Fluorescence Spectrophotometer (F2500). The fluorescence lifetimes of the samples were determined using an ultrafast time-resolved fluorescence spectrometer (Horiba FluoroMax Plus).

2.5 CCK-8 assay

A 96-well plate was prepared with each well containing 5000 Capan-1 cells, arranged in triplicates and categorized into blank, control, and experimental groups. PBS was added around the perimeter, and each well was filled with 100 μL of medium. On the second day, the cells were examined. The experimental group received various concentrations of POSS-QDs treatments. Subsequently, 10 μL of CCK8 reagent was added to each well. The plates were incubated at 37 °C for three hours, after which absorbance was measured at 450 nm.

2.6 Cell imaging

Capan-1 cells were plated and their morphology was observed on the second day. Various concentrations of POSS-QDs treatments were administered. After 24 hours, the slides were removed and washed three times with PBS. They were then fixed at room temperature with 4% paraformaldehyde for 15 minutes, followed by three additional PBS washes, each wash lasting 5 minutes.

3. Results and discussion

3.1 Synthesis and characterization of POSS-QDs

Fig. 1 presents a comprehensive schematic of the synthesis process for POSS/quantum dot composite nanoparticles. For SiQDs, this procedure initiates with the strategic combination of PEG-POSS, AEEA, and rose bengal. The mixture undergoes a high-temperature reaction within a specialized reactor to enable the *in situ* growth of SiQDs directly within the POSS

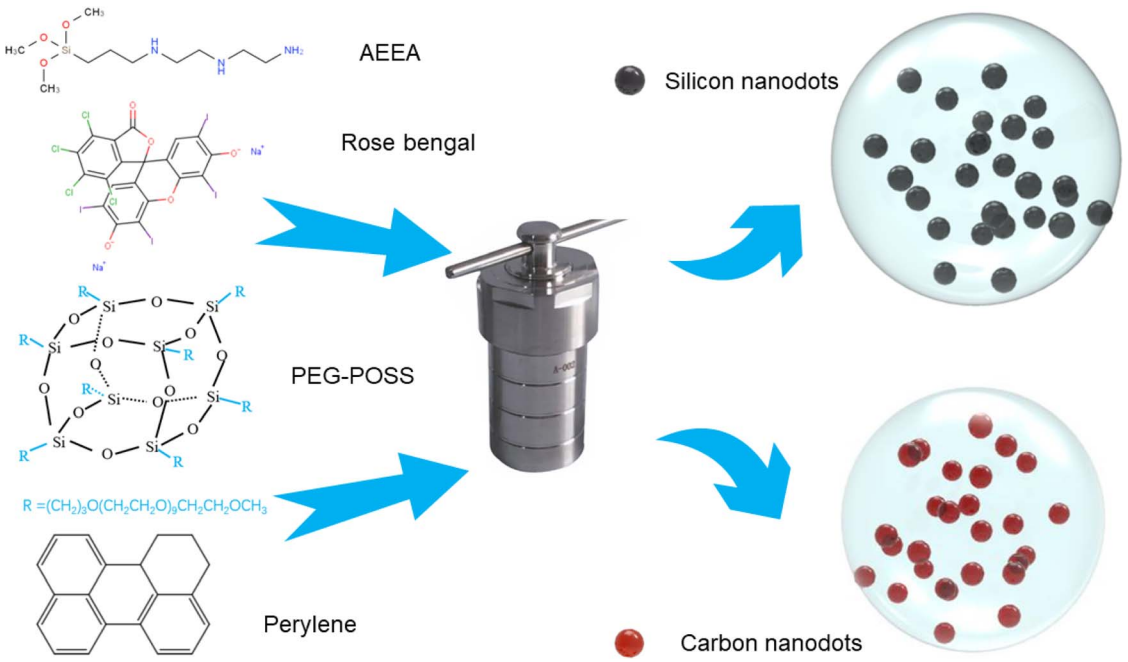

Fig. 1 Schematic diagram of the synthesis of POSS/quantum dot composite nanoparticles.

framework, yielding POSS-SiQDs. A crucial element of this synthesis is the interaction between the carboxyl groups of rose bengal and the amino groups of AEEA during hydrothermal treatment. This interaction is essential in the successful formation of silicon quantum dots.

In the production of the green POSS carbon quantum dots (POSS-G-CQDs),[25] the procedure involves the decomposition of PEG-POSS through a controlled heating process with a solution of perylene and $K_2S_2O_8$. This process is meticulously conducted at approximately 353 K to ensure optimal conditions for decomposition. Similarly, the creation of POSS-R-CQDs involves a high-temperature reaction of PEG-POSS with neutral red. These procedures underscore the precise control over the properties of the final product, demonstrating the versatility of POSS-based materials in the field of nanotechnology.

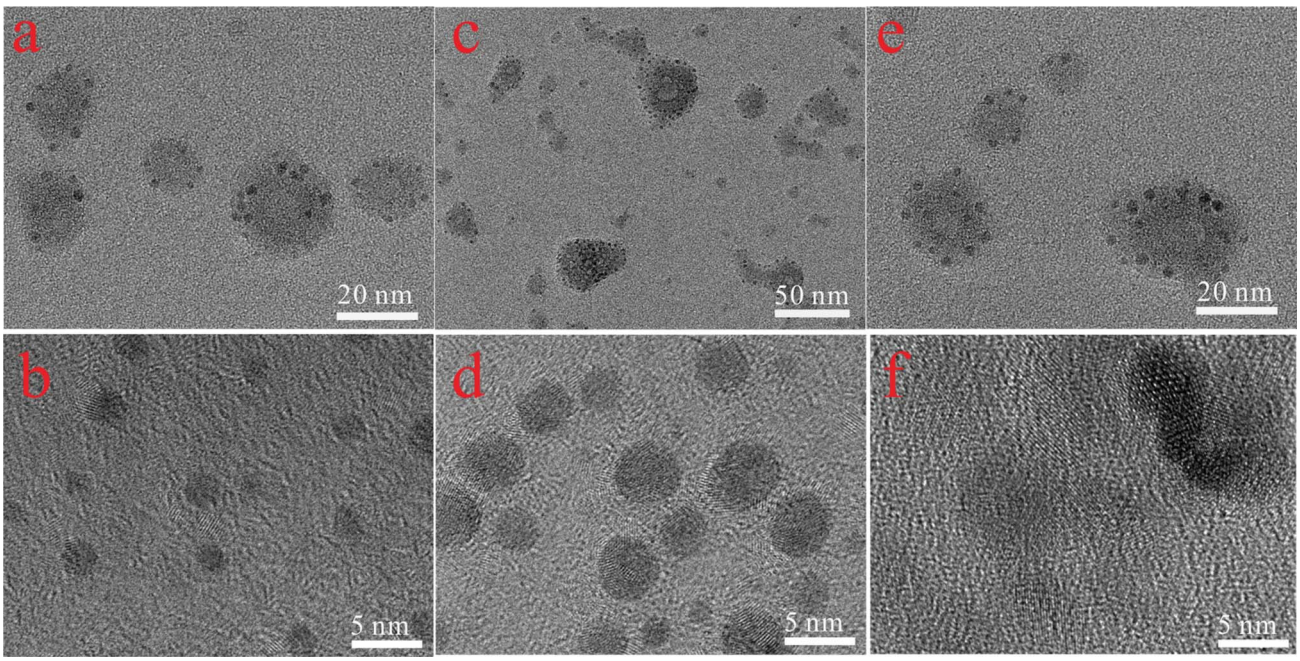

Fig. 2 (a and b) TEM and HR-TEM images of POSS-SiQDs; (c and d) TEM and HR-TEM TEM images of POSS-G-CQDs; (e and f) TEM and HR-TEM TEM images of POSS-R-CQDs.

The structural characterization of the purified POSS nanoparticles utilizes a suite of complementary techniques. Transmission Electron Microscopy (TEM) analysis reveals that the PEG-POSS particles are around 30–50 nm in size with a nearly spherical morphology (Fig. 2). Notably, SiQDs or CQDs are uniformly distributed within these spheres, highlighting the effective incorporation of quantum dots into the POSS framework. Detailed particle size analysis indicates that SiQDs have a diameter of 3.5 nm, while the CQDs present larger dimensions—G-CQDs at 4.5 nm and R-CQDs around 6 nm (Fig. S1–S3†). The challenge of centrifugal purification of such small-sized quantum dots is typically significant, often necessitating specialized treatments like dialysis. However, the incorporation of these quantum dots within the POSS particles significantly simplifies the centrifugal processing, reducing the need for high centrifugal forces. High-resolution characterization further elucidates the crystal lattice structure of these particles, providing a clear visualization of the lattice fringes and affirming the high-quality synthesis of these composite nanoparticles.

3.2 Optical properties of POSS-QDs

Fig. 3a and b illustrates the appearance of POSS-SiQDs, POSS-G-CQDs, and POSS-R-CQDs under ambient and ultraviolet light. Under ambient light, the solutions exhibit distinct colors: POSS-SiQDs appear yellow-brown, POSS-G-CQDs are green, and POSS-R-CQDs display a purple-red hue. When exposed to UV light (365 nm), these POSS composite particles emit strong fluorescence; POSS-SiQDs solution emit light blue, POSS-G-CQDs solution display green, and POSS-R-CQDs emit a red fluorescence. Fig. 3c is the UV-Visible absorption spectra for each type of POSS nanocomposite, highlighting their unique absorption peaks that reflect their specific electronic structures and interactions. The main absorption peak for POSS-SiQDs is at 280 nm, while POSS-G-CQDs exhibit an absorption peak at 323 nm, attributed to the n–π* transition of the C=O bond.[27] In contrast, POSS-R-CQDs have a prominent absorption peak at 400 nm.

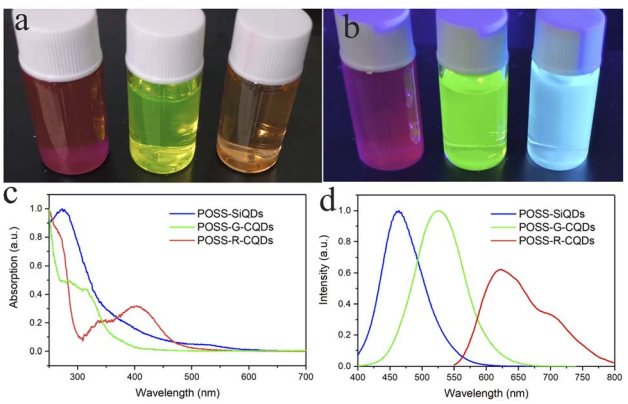

Fig. 3 (a and b) Photos of POSS-SiQDs, POSS-G-CQDs, and POSS-R-CQDs under ambient and ultraviolet light. (c) Absorption spectra of POSS-SiQDs, POSS-G-CQDs, and POSS-R-CQDs. (d) Emission spectra of POSS-SiQDs, POSS-G-CQDs, and POSS-R-CQDs.

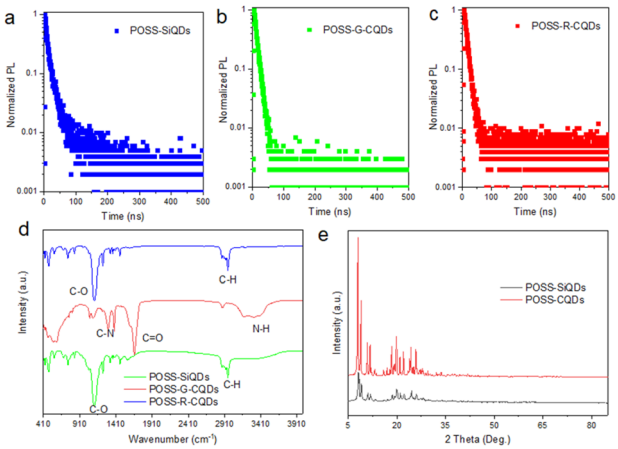

Fig. 4 (a–c) Fluorescence lifetime spectra of POSS-SiQDs, POSS-G-CQDs, and POSS-R-CQDs. (d) FTIR spectra of POSS-SiQDs, POSS-G-CQDs, and POSS-R-CQDs. (e) XRD spectra of POSS/SiQDs and POSS/CQDs.

Fig. 3d presents the fluorescence emission spectra: the emission center wavelengths are 450 nm for POSS-SiQDs and 530 nm for POSS-G-CQDs, with both PL curves following a Lorentzian distribution. The center emission wavelength for POSS-R-CQDs is approximately 625 nm. The detailed PL quantum yields (PLQYs) of the POSS-QDs and QDs are measured and listed in Table S1.† It demonstrates that due to the passivation strategy involving PEG-POSS, surface defects in SiQDs and CQDs were reduced, leading to increased PLQY. The solubility of these products in water and their stability at room temperature, combined with their intense fluorescence under UV light, highlight their potential for diverse applications in bioimaging and optoelectronics (Fig. 4).

Further analysing the PL characteristics of these POSS-QDs nanocomposites, we tested their fluorescence lifetime to verify whether they have a fast fluorescence recombination rate. The decay curves can be well fitted by a two-exponential-decay function

$$I(t) = I_0 + A_1 \exp\left(-\frac{t}{\tau_1}\right) + A_2 \exp\left(-\frac{t}{\tau_2}\right)$$

where τ_1 and τ_2 are the two characteristic lifetimes; A_1 and A_2 are their respective coefficients.[28] The total lifetime is $\tau = (A_1{\tau_1}^2 + A_2{\tau_2}^2)/(A_1\tau_1 + A_2\tau_2)$. The details of fitting parameter are listed in Table 1.

Fourier transform infrared spectroscopy (FTIR) was conducted to characterize the composites by identifying the functional groups present on their surface. As illustrated in the FTIR

Table 1 POSS-SiQDs, POSS-G-CQDs andPOSS-R-CQDs radiation recombination lifetime

	A_1	τ_1	A_2	τ_2	τ_{ave}
POSS-SiQD	0.49	12.47	0.51	2.79	10.64
POSS-G-CQDs	0.98	8.77	0.02	0.06	8.77
POSS-R-CQDs	0.92	9.22	0.08	1.28	9.12

spectra,[29] specific absorption peaks can be associated with particular chemical bonds within a molecule. The absorption peaks at 2950 cm^{-1} generally correspond to the stretching vibrations of C–H bonds in saturated hydrocarbons. The 1100 cm^{-1} peak is often associated with C–O stretching vibrations with the 1680 cm^{-1} peak corresponds to the stretching vibrations of C=O groups. The 600 cm^{-1} peak can be related to bending vibrations of bonds and the 1300 cm^{-1} peak indicates C–N stretching vibrations. These peaks indicate the presence of specific functional groups that are integral to the QDs' surface chemistry.

Moreover, the FTIR spectrum for SiQDs showcased two prominent peaks at 1611 cm^{-1} and 1465 cm^{-1}, which are ascribed to the vibrations of amide bonds. This specific observation underscores the presence of amide functionalities within the SiQDs structure, contributing to their unique chemical properties. The identification of these functional groups through FTIR analysis not only provides insight into the chemical composition and surface chemistry of the quantum dots and SiQDs but also suggests potential interactions and compatibility with various biological and chemical environments. This detailed characterization forms a foundational understanding of the materials properties, opening avenues for their application in fields ranging from nanotechnology to biomedicine, where the functional groups play a crucial role in determining the interaction with surrounding media. The XRD diffraction characterization of these powders revealed that the diffraction peaks within the 5–35° range predominantly reflect the characteristics of POSS-PEG.[30] The distinct XRD diffraction peaks confirm the high crystallinity of the synthesized composites.

3.3 Cell imaging of POSS-QDs

Before conducting cell imaging, we used the CCK-8 assay to evaluate the biocompatibility of the synthesized POSS-QDs.[31,32] The CCK-8 assay's high sensitivity, non-destructive nature, and simplicity allow for precise and continuous monitoring of the effects of POSS-QDs on cells. Specially, in CCK-8 assay, we detected the reduction of WST-8 to formazan by cellular dehydrogenases, which directly indicates cell health. The results revealed that the cell survival rate is around 80%, indicating that the POSS-QDs we synthesized have good biocompatibility, which can be fluorescent probe candidate for cell imaging.

For cell images, Capan_1 cells were incubated in a culture medium infused with POSS-QDs at a concentration of 0.02 mg mL^{-1} for 20 minutes. Upon exposure to an excitation wavelength, their laser confocal fluorescence imagery was captured within the ultraviolet light spectrum (395–415 nm). The findings revealed that Capan_1 cells exhibited vivid fluorescence in blue, green, and red when tagged with POSS-SiQDs, POSS-G-CQDs, and POSS-R-CQDs, respectively, as depicted in Fig. 5. The efficiency of POSS/QDs in traversing cell membranes and illuminating cell interiors with bright colors under UV light underscores their significant potential as a versatile tool in biological and medical investigations. The intense and distinct fluorescence demonstrated by cells treated with POSS/QDs

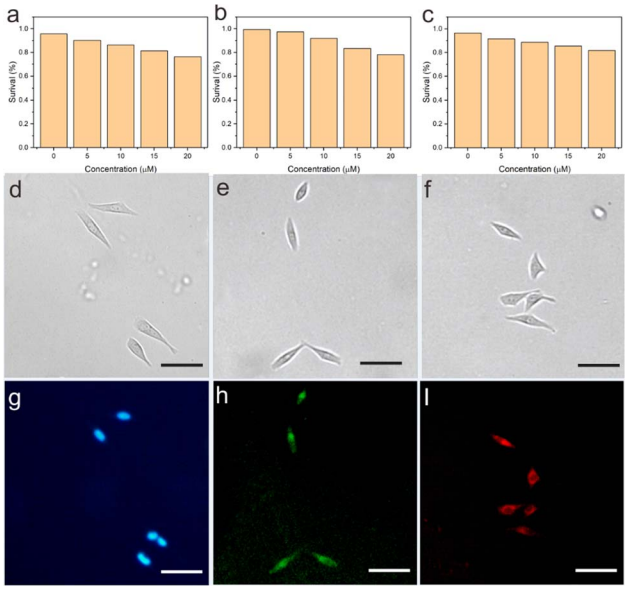

Fig. 5 (a–c) The CCK-8 assay results, (d–f) bright field and (g–i) cell imaging using POSS-SiQDs, POSS-G-CQDs and POSS-R-CQDs, the scale bar is 20 μm.

accentuates the robust luminescent properties of POSS/QDs, positioning them as prime candidates for intricate biological imaging endeavors. These results confirm the biocompatibility and cellular penetration capability of POSS-QDs, allowing them to easily enter cells and demonstrate fluorescence imaging. This makes POSS-QDs highly suitable for multicolor cell imaging analyses in living cells, highlighting their potential for internal multicolor imaging applications.

It is reasonable to expand the scope of POSS-QDs to explore additional potential applications, such as targeted drug delivery and therapeutic agents, which could significantly enhance its impact. The functionalization potential of these nanocomposites allows for the attachment of specific ligands or antibodies that target particular cells or tissues. This specificity can be utilized in targeted drug delivery systems, where the nanocomposites deliver therapeutic agents directly to diseased cells, minimizing side effects on healthy tissues. The biocompatibility and adjustable biodegradability of POSS nanocomposites make them suitable candidates for therapeutic applications.

4. Conclusion

In summary, we *in situ* synthesized POSS-SiQDs, POSS-G-CQDs, and POSS-R-CQDs, which emit blue, green, and red light, respectively. The unique structure of POSS encapsulates and protects the QDs, resulting in POSS-QDs that exhibit high PLQY, adequate stability, and rapid fluorescence decay properties. Additionally, these materials demonstrate good biocompatibility and efficient cellular membrane penetration. These features ensure their applicability in facilitating multicolored intracellular imaging, enabling detailed visualization of various cellular components and processes in vibrant colors, thereby

enriching the quality and detail of biological imaging studies. Our *in situ* synthesis strategy unveils new horizons for the preparation of SiQDs and CQDs, opening new pathways for exploration and innovation of QDs in biological imaging and medical diagnostics.

Data availability

Data for this article are available at **https://zenodo.org/records/12677235**

Conflicts of interest

There are no conflicts to declare.

Acknowledgements

This work is supported by Anhui Province Key Research and Development Plan Project (No. 2022e07020066).

References

1 S. Terada, Y. Xin and K.-i. Saitow, *Chem. Mater.*, 2020, **32**, 8382–8392.
2 L. Tian, Z. Li, P. Wang, X. Zhai, X. Wang and T. Li, *J. Energy Chem.*, 2021, **55**, 279–294.
3 M. J. Molaei, *Anal. Methods*, 2020, **12**, 1266–1287.
4 L. Wang, W. Li, L. Yin, Y. Liu, H. Guo, J. Lai, Y. Han, G. Li, M. Li and J. Zhang, *Sci. Adv.*, 2020, **6**, eabb6772.
5 Ł. Janus, J. Radwan-Pragłowska, M. Piątkowski and D. Bogdał, *Materials*, 2020, **13**, 3313.
6 P. Jana and A. Dev, *Mater. Today Commun.*, 2022, 104068.
7 Y. Zhang, N. Cai and V. Chan, *Biosensors*, 2023, **13**, 311.
8 N. Wei, Y.-C. Sun, X.-F. Guo and H. Wang, *Microchim. Acta*, 2022, **189**, 329.
9 A. K. Subramania, D. K. Maurya, M. Saikia, R. D. Navaneethan and S. Angaiah, *Mater. Adv.*, 2023, **4**, 3951–3966.
10 V. B. Kumar, I. Sher, S. Rencus-Lazar, Y. Rotenstreich and E. Gazit, *Small*, 2023, **19**, 2205754.
11 R. Ramasubburayan, K. Kanagaraj, L. Gnanasekaran, N. Thirumalaivasan and N. Senthilkumar, *Waste Biomass Valorization*, 2024, 1–10.
12 R. Yıldırım, M. S. Ullah, H. R. Koçoğlu, M. Ün, N. Yazıcı Çakır, G. l. a. Demir, D. Çetin, G. Urtekin, G. r. Özkoç and O. Mert, *ACS Omega*, 2023, **8**, 47034–47050.
13 J. K. R. Modigunta, K. N. Park, S. C. Shin, G. Murali, U. H. Haran, J. Kim, J. Yeon, S. Park, H. Jang and Y. H. Park, *J. Energy Storage*, 2023, **74**, 109344.
14 J. Rezaie, N. Jabbari, S. A. Kalashani, E. Jabbari and A. Akbari, *Mater. Lett.*, 2022, **307**, 131013.
15 W. J. Kim, E. H. Lee, Y.-J. Kwon, S.-K. Ye and K. oh Kim, *RSC Adv.*, 2022, **12**, 18209–18214.
16 M. Feghhi, J. Rezaie, A. Akbari, N. Jabbari, H. Jafari, F. Seidi and S. Szafert, *Mater. Des.*, 2021, **197**, 109227.
17 J. Ozimek and K. Pielichowski, *Molecules*, 2021, **27**, 40.
18 L. Wang, Z. Du, M. Xu, Q. Dai, Q.-Y. Guo, B. Fan and W. Tang, *Biomacromolecules*, 2023, **24**, 5071–5082.
19 C. Kurtulus, M. Kuyumcu, M. Ciftci and M. A. Tasdelen, *Polym. Compos.*, 2021, **42**, 4056–4064.
20 M. S. Stan, L. O. Cinteza, L. Petrescu, M. A. Mernea, O. Calborean, D. F. Mihailescu, C. Sima and A. Dinischiotu, *Sci. Rep.*, 2018, **8**, 5289.
21 G. Soufi, H. Bagheri, L. Y. Rad and S. Minaeian, *Anal. Chim. Acta*, 2022, **1198**, 339550.
22 Ł. John, M. Malik, M. Janeta and S. Szafert, *RSC Adv.*, 2017, **7**, 8394–8401.
23 P. Loman-Cortes, T. Binte Huq and J. L. Vivero-Escoto, *Molecules*, 2021, **26**, 6453.
24 X. Chen, X. Zhang, L.-Y. Xia, H.-Y. Wang, Z. Chen and F.-G. Wu, *Nano Lett.*, 2018, **18**, 1159–1167.
25 T. Yuan, F. Yuan, L. Sui, Y. Zhang, Y. Li, X. Li, Z. a. Tan and L. Fan, *Angew. Chem.*, 2023, **135**, e202218568.
26 A. Madonia, G. Minervini, A. Terracina, A. Pramanik, V. Martorana, A. Sciortino, C. M. Carbonaro, C. Olla, T. Sibillano and C. Giannini, *ACS Nano*, 2023, **17**, 21274–21286.
27 E. E. Ateia, O. Rabie and A. T. Mohamed, *Eur. Phys. J. Plus*, 2024, **139**, 24.
28 Y. Wang, X. Li, J. Song, L. Xiao, H. Zeng and H. Sun, *Adv. Mater.*, 2015, **27**, 7101–7108.
29 C. Liu, F. Zhang, J. Hu, W. Gao and M. Zhang, *Front. Chem.*, 2021, **8**, 605028.
30 R. Venkatesan, R. Vanaraj, K. Alagumalai, S. P. Asrafali, C. J. Raorane, V. Raj and S.-C. Kim, *Antibiotics*, 2022, **11**, 1425.
31 X. Song, X. Zhang, Q. Xia, C. Li, Y. Zhang, Y. Huang, L. Meng, C. Wang, J. Li and W. Long, *J. Clin. Lab. Anal.*, 2023, **37**, e24802.
32 S. Chen, R. Zhao, X. Sun, H. Wang, L. Li and J. Liu, *Adv. Healthcare Mater.*, 2023, **12**, 2201924.